Electronic Supplementary Information

On the interplay of shell structure with low and high-frequency mechanics of multifunctional magnetic microbubbles

Melanie Poehlmann[a], Dmitry Grishenkov[b,c], Satya V.V.N. Kothapalli[b], Johan Harmark[d,e], Hans Hebert[d,e], Alexandra Philipp[a], Roland Hoeller[a], Maximilian Seuss[a], Christian Kuttner[a], Silvia Margheritelli[f], Gaio Paradossi[f], Andreas Fery*[a]

1. Determination of the attenuation coefficient:

The attenuation coefficient of the ultrasound wave propagating through the MBs suspension is determined using a two-time.-domain signals. The first signal is acquired from the ultrasound pulse propagating through the cell filled with pure water. The second signal is collected from the cell filled with the suspension of the MBs. The Fourier analysis reveals the harmonic decomposition of the time-domain signals to be equal:

$$f_{\text{ref}}(t) = \frac{1}{2\pi}\int_{-\infty}^{\infty}|F_{\text{ref}}(\omega)|\, e^{-jk_{\text{ref}}z} e^{-j\omega t} d\omega \tag{1}$$

Where $|F_{\text{ref}}(\omega)|$ and $k_{\text{ref}}z$ are modulus and phase of the spectra acquired from pure water. If the dissipation of energy is added, due to wave propagation through the MBs suspension, the only effect it cause is that the wave vector $\vec{k}$ becomes complex, *i.e.* $k_{\text{MB}}(\omega) = k_1(\omega) - jk_2(\omega)$. Thus, the spectrum of the signal from MBs can be rewritten as:

$$f_{\text{MB}}(t) = \frac{1}{2\pi}\int_{-\infty}^{\infty}|F_{\text{MB}}(\omega)|\, e^{-jk_{\text{MB}}(\omega)z}\, e^{-j\omega t} d\omega =$$

$$= \frac{1}{2\pi}\int_{-\infty}^{\infty}|F_{\text{ref}}(\omega)|\, e^{-[k_2(\omega) - jk_1(\omega)]z}\, e^{-j\omega t} d\omega \tag{2}$$

Where $k_2(\omega)$ should be seen as attenuation coefficient $\alpha(\omega)$, and wave number $k_1(\omega)$ represents the phase shift. Taking into account the "round-trip" propagation of the beam through the cell of length L, the harmonic decomposition of the signal from MBs on its final form is:

$$f_{\text{MB}}(t) = \frac{1}{2\pi}\int_{-\infty}^{\infty}|F_{\text{ref}}(\omega)|\, e^{-[\alpha(\omega) - jk_1(\omega)]2L}\, e^{-j\omega t} d\omega \tag{3}$$

Substituting the scale from Np to dB, the attenuation coefficient $\alpha(\omega)$, can be calculated from:

$$\alpha(\omega) = -\frac{20}{2\text{L}}\log\left(\frac{|F_{\text{MB}}(\omega)|}{|F_{\text{ref}}(\omega)|}\right) {}^{\text{dB}}/_{\text{unit length}} \tag{4}$$

2. Atomic force microscopy - Characterization of diameter and shell thickness

Table S1: Summary of the results from the statistical analysis of the AFM height images: diameter *d*, shell thickness *H* with the corresponding standard deviation (SD), and half-width at half maximum (HWHM).

Parameter	*n*	Median ± SD	Gauss ± HWHM	SD Gauss = HWHM/√2
$d_{\text{AFM,dry}}$ (µm)	203	3.7 ± 0.9	3.5 ± 1.12	0.8
$H_{\text{AFM,dry}}$ (nm)	158	171 ± 68	152 ± 90	63
$H_{\text{AFM,water}}$ (nm)	36	249 ± 127	215 ± 133	94

3. Transmission electron microscopy - characterization of shell thickness

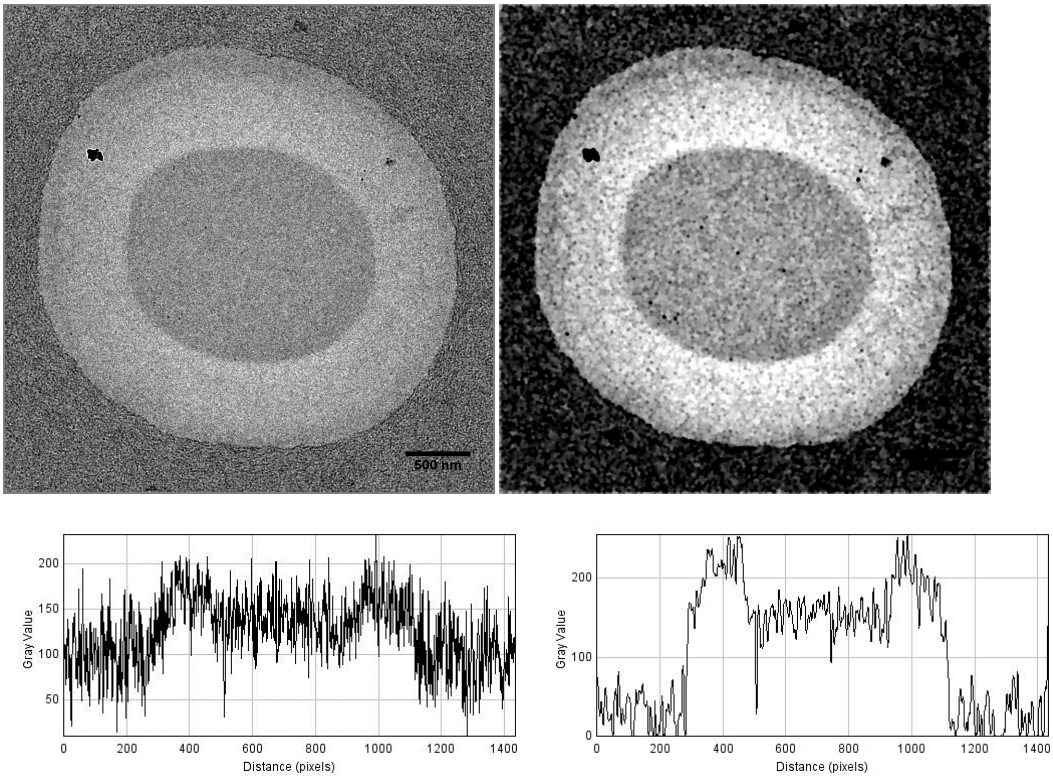

Figure S2: For the cross-sectional profiles an enhanced contrast was needed to evaluate the images with an standardized protocol using ImageJ[1]. Protocol: Filter Minimum (2 pixels + adjust B&C);enhance contrast 0.35 + adjust B&C; Filter Maximum (2 pixels + adjust B&C); enhance contrast 0.35 + adjust B&C, repeat this procedure and plot a profile from the lower left to upper right corner. Thus, we were able to identify the PVA/EPON interface at ±50% change of the gray scale value.

4. Mathematical procedure of random slicing correction

True thickness H of the capsule wall is given by the difference of the true outer R and inner radius r at the equatorial plane (see Figure S3). All measured sizes are indicated by an index i and are affected by the position, where the capsule is sectioned for TEM. For random slicing, the both radii are underestimated ($\langle R_i \rangle \leq R, \langle r_i \rangle \leq r$) and the wall thickness is overestimated ($\langle H_i \rangle = \langle R_i - r_i \rangle \geq H$). In the following, radii are always considered as pairs ($N_{R_i} = N_{r_i}$), since these values are correlated. The angle of the outer radius Φ is limited between $[-\Phi_{\text{limit}}, +\Phi_{\text{limit}}]$ with $\Phi_{\text{limit}} = \sin^{-1}\big((R-H)/R\big) = \pi/2 - \sin^{-1}(-H/R)$, where the angle of the inner radius ϕ is not limited ($[-\pi/2, +\pi/2]$).

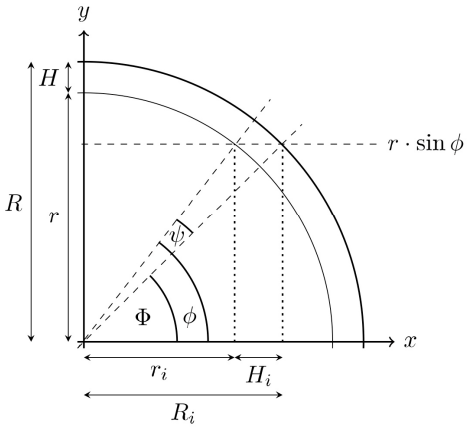

Figure S3: Definition of geometry of a sphere of uniform thickness used in the mathematical analysis that corrects for random slicing along the *y*-axis during TEM sample preparation.[2]

The assumption is that if we have good statistical data, we can apply a mathematical correction introduced by Smith *et al.* to calculate the true values.[2] This approach is based on a geometrical function $H(R_i, H_i, \Phi)$ and $\psi = \phi - \Phi$.

$$H = \left(\frac{R_i}{\cos(\Phi)}\right) - \sqrt{H_i^2 - \left(\frac{R_i}{\cos(\Phi)}\right)^2 + 2R_i\left(\frac{R_i - H_i\cos^2(\Phi)}{\cos^2(\Phi)}\right)} \tag{5}$$

The mean corrected thickness $\langle H \rangle$ is then given by a triple integral:

$$\langle H \rangle = \int_{-\Phi\,\text{limit}}^{+\Phi\,\text{limit}} \int_{H_{i,\min}}^{H_{i,\max}} \int_{R_{i,\min}}^{R_{i,\max}} H\,(R_i, H_i, \Phi)\, f_R(R_i) f_H(H_i) f_\Phi(\Phi)\, dR_i\, dH_i\, d\Phi \tag{6}$$

The functions f_R, f_H, and f_Φ are the normalized probability density functions of R_i, H_i, and Φ, respectively. If f_R and f_H (obtained from the statistics of the image analysis data) are normally distributed then they can be described by Gaussian distributions (mean and standard deviation).

Smith *et al.* assumed that if there is an equal probability of slicing at any angle Φ then $f_{\Phi,\text{Smith}}(\Phi) = 1/\pi$.[2] Mercade-Prieto et al. reported that this assumption is incorrect since this would mean, that there is an equal probability to cut from 0° to 45° and from 45° to 90°.[3] They suggested that the distance from the equator ($r\sin(\phi)$ or $R\sin(\Phi)$) should be the parameter of equal probability. Therefore we introduced a new probability density function $f_{\Phi,\text{new}} = 0.5\cos(\Phi)$. Table S4 compares the old and new function f_Φ.

Table S4: Comparison of the angular probability density function and integrations for different angular ranges.

Angular range	-90° to 90°	0° to 45°	45° to 90°
Integration	$\int_{-\pi/2}^{+\pi/2} f_\Phi\, d\Phi$	$\int_{0}^{+\pi/4} f_\Phi\, d\Phi$	$\int_{+\pi/4}^{+\pi/2} f_\Phi\, d\Phi$
$f_{\Phi,\text{Smith}}(\Phi) = 1/\pi$	1	0.25	0.25
$f_{\Phi,\text{new}} = 0.5\cos(\Phi)$	1	0.35	0.15

The corrected inner radius r is given by:

$$\langle r_i \rangle = \int_\phi \int_r r_i\; f_r(r)\; f_\phi(\phi)\, dr\, d\phi \tag{7}$$

The measured radius r_i can be substituted by $r\cos(\phi)$. If r and ϕ are independent, the integrals can be separated. Using f_ϕ and integrating over ϕ and r yields the correction factor of the inner radius.

$$\langle r_i \rangle = \int_{-\frac{\pi}{2}}^{+\frac{\pi}{2}} \cos(\phi)\, f_\phi(\phi)\, d\phi \;\; \int_0^r r\, f_r(r)\, dr \tag{8}$$

$$\langle r_i \rangle = \frac{\pi}{4}\langle r \rangle \tag{9}$$

The mean corrected outer radius $\langle R \rangle$ can be calculated from the following equation:

$$\langle R \rangle = \frac{4}{\pi}\left(\langle R_i \rangle - \langle H_i \rangle\right) + \langle H \rangle \tag{10}$$

Since solid disks (slicing inside of the capsule wall) were excluded from the statistical analysis, the integration of Φ is limited. This limit is given by

$$\Phi_{\text{limit}} = \sin^{-1}\left(\frac{\langle R \rangle - \langle H \rangle}{\langle R \rangle}\right) \tag{11}$$

Solution procedure: [2]

1.) Determine mean and standard deviation for R_i and H_i from the TEM data. Only include data pairs of R_i and r_i. Exclude solid discs.
2.) Guess Φ_{limit}.
3.) Solve for $\langle H \rangle$ by integration within ± 4 standard deviation of R_i and H_i.
4.) Solve for $\langle R \rangle$.
5.) Check whether $\Phi_{\text{limit}}(\langle R \rangle, \langle H \rangle)$ is satisfied. If not, repeat from step 3-5 using new Φ_{limit}.

5. Acoustic Modeling

As Table 3 indicates, the concentration is less important for plain MBs and MBs-phys than for MBs-chem. MBs-chem appear to be more sensitive to the variation of the concentration. Even though the static terms of both viscoelastic moduli, G_{eq} and μ_0, seems to be consistent among all concentration values the dynamic terms, G_1 and μ_1, are different. For instance, at low concentration μ_1 is approaching zero, while at high concentration G_1 can be neglected. The possible explanation of this phenomenon might be found in the experimental set-up itself. In particular, for assessment of the attenuation coefficient the ultrasound probe at a central frequency of 10 MHz was employed. The frequency of the probe matches the resonance frequency of the MBs-chem. As a result, maximum radial expansion of the bubble occurs; scattering intensity of the wave is increased by several folds compare to the one predicted by Rayleigh scattering model[4] at high concentration (typically above 10^6 MB/mL) multiple scattering and reradiation of the waves might occur in the suspension[5]. In addition, it was reported by de Jong *et al.,*[6] that MBs driven within 10% of their resonance frequency generate strong nonlinear harmonic response. Keeping in mind that linearized theoretical model accounts only for small oscillations around equilibrium, and consider only fundamental response, the frequency dependent or dynamic terms probably are not correctly assessed, while frequency independent or static terms are still possible to recover. This is in line with the fact that de Jong and Hoff[7] manage to predict sharp resonance peak for thin shelled Albunex® or Sonazoid® bubble using frequency independent shear modulus G, and viscosity μ_0 at about 2 and 4 MHz respectively. Worth to be noted is that plain MBs and MBs-phys oscillate far from their resonance and modified theoretical model manages to predict the attenuation profile with one set of coefficients for all concentrations. Worth noting that dynamic storage and loss modulus are characteristics of the shell material itself, but not the suspension of the MBs in general. As a result dynamic viscoelastic moduli should be independent on the microbubble concentration if multiple reradiation of energy, multiple scattering, interaction between the MBs and resonance are disregarded.

1. C. A. Schneider, W. S. Rasband and K. W. Eliceiri, *Nat Meth*, **9**, 671-675.
2. A. E. Smith, Z. Zhang and C. R. Thomas, *Chem. Eng. Sci.*, 2000, **55**, 2031-2041.
3. R. Mercade-Prieto, B. Nguyen, R. Allen, D. York, J. A. Preece, T. E. Goodwin and Z. B. Zhang, *Chemical Engineering Science*, 2011, **66**, 2042-2049.
4. N. de Jong, F. J. Ten Cate, C. T. Lancée, J. R. T. C. Roelandt and N. Bom, *Ultrasonics*, 1991, **29**, 324-330.
5. E. Stride and N. Saffari, *IEEE Trans. Ultrason. Ferroelectr. Freq. Control*, 2005, **52**, 2332-2345.
6. N. de Jong, R. Cornet and C. T. Lancée, *Ultrasonics*, 1994, **32**, 447-453.
7. N. de Jong, L. Hoff, T. Skotland and N. Bom, *Ultrasonics*, 1992, **30**, 95-103.